

Advanced Simulation of the Flow and Heat Transfer Processes in Simultaneous Engineering

M. R. Barkhudarov

Flow Science, Inc., 1257 40-th Street, Los Alamos, New Mexico 87544, USA

Tel: +1-505-662-2636, Fax: +1-505-662-6564, e-mail: mike@flow3d.com

Abstract

A brief discussion of basic approaches to numerical modeling of liquid metal flow and heat transfer is given followed by a number of casting simulation examples. These examples demonstrate how numerical modeling can be used and what can be learnt from the simulation results. The examples are based on using a commercial, general purpose, CFD code *FLOW-3D*[®].

Introduction

Numerical modeling provides a powerful means of analyzing various physical phenomena occurring during casting processes. It gives an insight into the details of fluid flow, heat transfer and solidification. Numerical solutions allow researchers to observe and quantify what is not usually visible or measurable during real casting processes. The goal of such simulations is to help shorten the design process and optimize casting parameters to reduce scrap, use less energy and, of course, make better castings.

Simulation produces a tremendous amount of data that characterize the transient flow behavior (*e.g.*, velocity, temperatures), as well as the final quality of the casting (*e.g.*, porosity, grain structure). It takes good understanding of the actual casting process, and experience in numerical modeling, for a designer to be able to relate one to the other and derive useful conclusions from the results.

Modeling Approaches

Most of the casting modeling codes can be divided into two categories: those using the finite difference (FD) approach for solving fluid flow equations, and those that employ the finite element (FE) method. The FE method uses body-fitted computational grids leading to more accurate representation of metal/mold interfaces than generally achievable by FD methods (Fig 1). However, generating good quality FE grids is still a challenging task and often takes significantly more time than the simulation itself. Solution accuracy degenerates in highly distorted grids and changes in geometry, even small ones, often require a completely new grid.

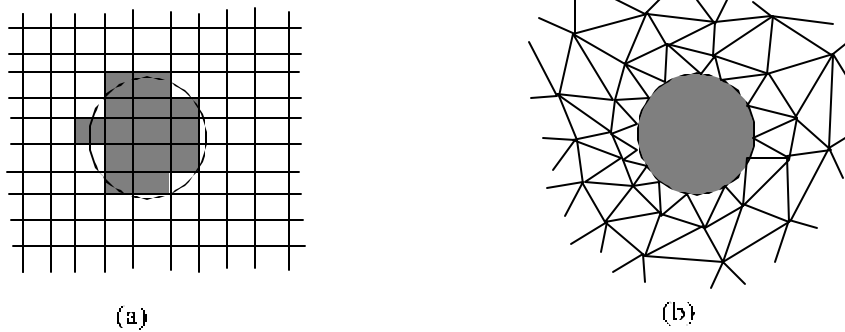


Figure 1. Typical finite difference (a) and finite element (b) mesh resolution of a circular object..

The FD method offers ease of mesh generation due to the structured nature of the mesh, uses less storage to describe geometry and simplifies the implementation of the numerical algorithms. However, the conventional FD methods often require fine grids to describe complicated geometry to reduce errors associated with the ‘stair-step’ representation of curved boundaries. The latter introduces inaccuracies when computing liquid metal flow along the walls and heat fluxes normal to the walls.

An advancement of the conventional FD method is given by the Fractional Area/Volume Obstacle Representation (FAVOR) method. In this method rectangular grid cells can be partially blocked by obstacles [1]. The blockage is described by using fractional cell volumes and areas on cell sides as shown in Fig. 2a. The FAVOR method improves the accuracy of the numerical solution near mold walls and allows for the use of coarser grids than in standard FD methods (see example in Fig. 2b). Since the geometry representation is less mesh-dependent, the FAVOR method is also referred to as a ‘free gridding’ method.

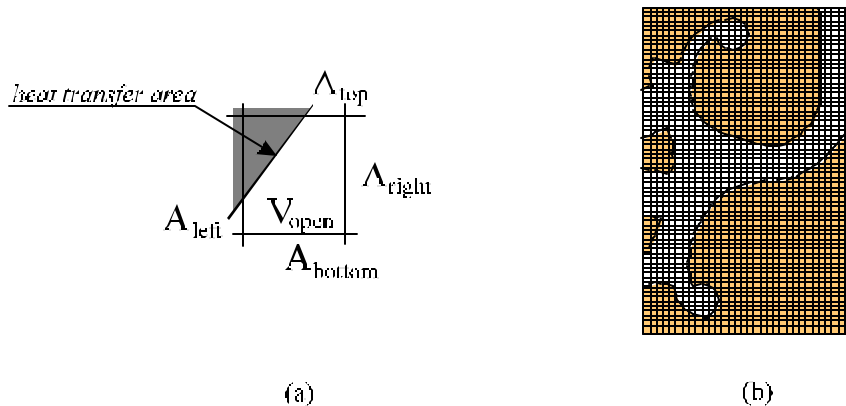


Figure 2. The partial cell (FAVOR) method to describe geometry in a 1D grid. Definition of the open area and volume fractions (a), with a runner and system example resolution (b).

Mold filling problems involve tracking free surfaces that are the boundaries between liquid metal and the surrounding air. The most commonly used method to describe free surfaces is the Volume-of-Fluid (VOF) method. The VOF method enables the tracking the transient free surfaces with arbitrary topology and deformations (*e.g.*, fluid surface breakup and coalescence). The ‘true’ VOF method consists of three main components [2]:

- A fluid fraction function $F(t, \mathbf{r})$ which is equal to 1.0 in fluid regions, and equal to 0.0 in voids. Since fluid configurations may change with time, F is a function of time, t , as well as space, \mathbf{r} . Averaged over a computational control volume, the fluid fraction function has a fractional value in cells containing a free surface as shown in Fig. 3.
- Zero shear stress and constant pressure boundary conditions are applied at free surfaces.
- A special advection algorithm is used for tracking sharp free surfaces.

A free-surface advection method must preserve the sharpness of the interface and have minimal free surface distortion. Generally, such advection algorithms are based on geometric reconstruction of the free surface using the values of F at grid nodes [3].

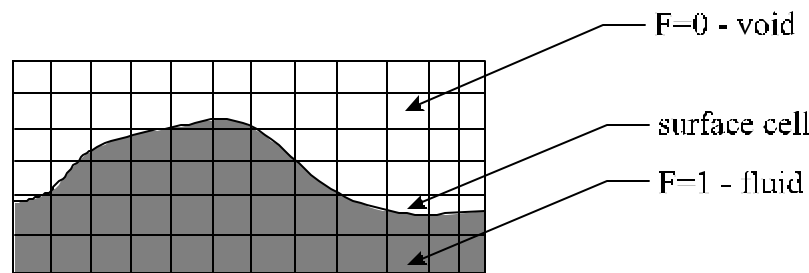


Figure 3. Volume-Of-Fluid (VOF) function definition.

Sometimes a free surface is approximated by a density discontinuity between metal and air and flow equations are solved for both fluids. In that case it is difficult to enforce correct boundary conditions at the surface. This is because free surface pressure and velocities in the two-fluid approach are not set explicitly, but are computed by solving the flow equations and these flow equations are solved in terms of mixture variables. Since densities of liquid metal and air differ greatly (*e.g.*, by a factor of 7,000 for steel), the mixture velocity may not always be an accurate measure of the relative motion of metal and air. An example of such a case is shown in Fig. 4 where liquid metal (aluminum) is filling a rectangular box with an open riser at the top. In the two-fluid simulation the metal is unrealistically drawn into the riser by the escaping air before the cavity is full, in contrast to the one-fluid simulation where the cavity is full before the metal enters the riser.

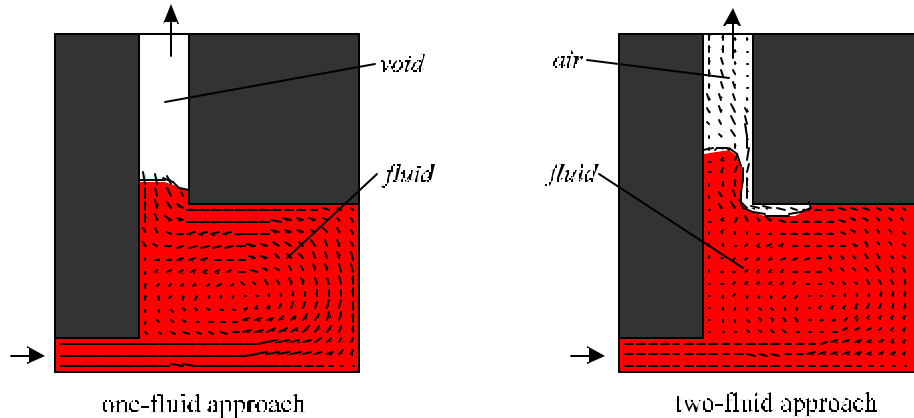


Figure 4. Simple mold filling simulation using the VOF function to describe the metal location: (a) one-fluid model, (b) two-fluid model with one mixture velocity per cell.

Numerical solution of the basic fluid flow and heat transfer equations produces spatial distributions of pressure, velocity and temperature at each incremental time step. Other physical models can be added using these basic quantities: *e.g.*, phase transformation, flow losses in filters, porosity formation, non-Newtonian effects and so on. These models can then be combined to model a variety of casting processes.

The main considerations when preparing a simulation are:

- What is to be learned from the simulation?
- What physical processes are important and, therefore, should be included in the model?
- Is the computational tool appropriate for the analysis?

Answering these questions before starting a simulation helps to get the results in the most efficient way. For example, if the interest is only in fluid flow, then heat transfer may be turned off.

Useful things can often be learnt from simple models. For example, two-dimensional simulations are easy to visualize and understand and can be used to quickly test different modeling assumptions and perform sensitivity studies. Initial 3-D runs can be carried out with a coarse grid to verify the numerical model. All in all, these test runs help the user to build up confidence in the chosen modeling approach.

Simulation Examples

All numerical examples below are obtained using a commercial, general-purpose CFD package *FLOW-3D*[®] [4]. *FLOW-3D* is based on a control volume/finite difference approach. Free

surfaces are tracked using the VOF algorithm, which together with the FAVOR method, is incorporated into the Navier-Stokes equations of fluid motion.

1. Simple Gating Examples

Three gating configurations were tested in a series of 2-D simulations: bottom gating, side gating and top gating. In each case there are two gates connecting a straight runner to a $200 \times 300 \text{ mm}$ rectangular box. The runner inlet velocity is 100 mm/sec with the filling time of 2.5 sec . Assuming that we are casting aluminum, we will concern ourselves with the goal of a smooth filling process and a minimal air entrapment. Excessively turbulent flow with a lot of splashing may lead to an entrapment of surface oxides that result in mechanical weaknesses in the solidified casting [5]. We will not consider the effects of heat transfer during filling.

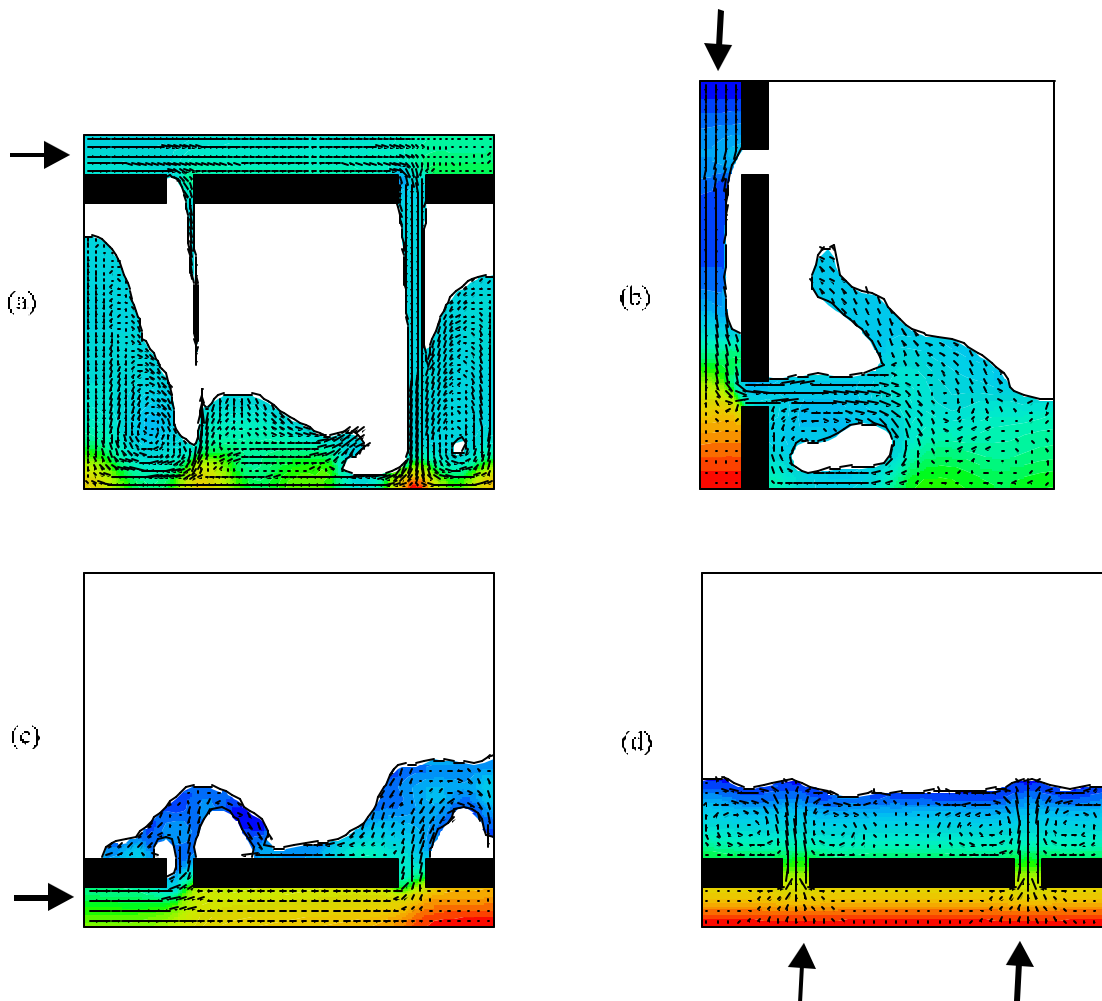


Figure 5. Filling pattern for (a) top gating, (b) side gating, (c) bottom gating design with fixed flow rate. Example (d) shows bottom-gated low pressure filling. Colors represent pressure.

Figure 5a shows the liquid metal flow for the ‘top gating’ design. Inertia carries metal past the first gate so that the metal enters the cavity mostly through the gate that is farthest from the inlet. The incoming metal accelerates during its free fall in the cavity resulting in significant splashing. The splashing and air entrapment continues until the box is almost full. Such gating system produces perhaps the worst filling scenario.

The ‘side gating’ design is shown in Fig. 5b. An interesting feature of this filling pattern is the flow through the top gate. Instead of metal entering the cavity, air is being sucked into the runner through the gate. Large air bubbles form in the runner, which is then carried down by the flowing metal to the lower gate, where the metal/air mixture enters the cavity with a splash. The latter adds to the air entrapment that occurs in the runner. Air entrapment is reduced towards the end of the filling, when the gates become submerged in liquid metal, but the damage is already done by that time.

Figure 5c shows the ‘bottom gating’ design. In this case the flow is turbulent primarily during the initial stage of filling, when metal jets up through the gates into the cavity. At later stages, when there is enough fluid in the cavity to damp the energy of the incoming flow, the filling is smoother. As in the ‘top gating’ case, there is more metal flowing through the gate farthest from the inlet.

The final simulation was carried out for the ‘bottom gating’ configuration, but with pressure rather than fixed velocity controlling the filling rate (low pressure, or counter-gravity, filling). Lowering the pressure in the cavity to 5% below the atmospheric pressure over the time of 10 *sec*, produces very smooth filling pattern as shown in Fig. 5d. Of course, with such relatively long filling time there may be problems with cold shuts, but that is a matter of another investigation.

2. High Pressure Die Casting

In this example the geometry has a complicated 3-D shape of an alternator housing that is currently produced by General Motors [6]. The geometry of the part and the runner/gating system was defined as a stereolithography (STL) object and imported into the preprocessor (Fig. 7). The filling time is 65 *msec*, which translated into a runner inlet velocity of 15.5 *m/sec*. We will look at the flow uniformity in the gating system, filling pattern during high pressure injection of liquid metal (aluminum) and the thermal solution in the metal and die (H13 steel). In the latter case the die geometry and cooling channels must be included. The die has two cavities, but taking advantage of their symmetric location, only half of the total casting was modeled.

Initially, we analyze the flow in the runner/gating system by allowing the metal run freely through the three gates. The flow pattern and velocity histories in each gate are shown in Fig. 6. There are two interesting points to note. First, the flow velocities are not the same in the three gates. In fact, the velocity in the top gate in Fig. 6 is about 20% smaller than in the other two gates. Secondly, there is flow separation occurring in the top gate resulting in a part of its cross-section

running 'dry'. Smoothing the corner upstream from the separation region may help achieve better flow efficiency in this gate.

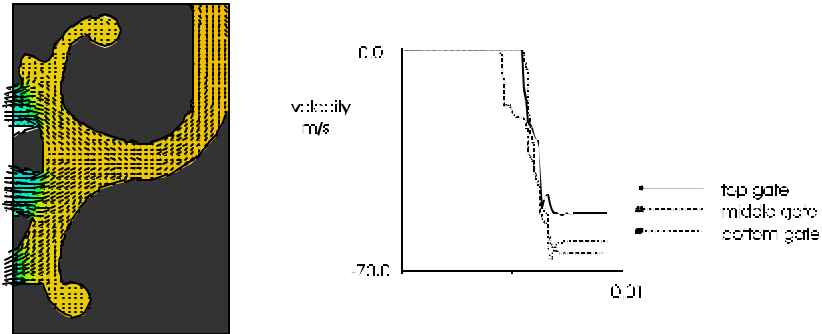


Figure 6. Liquid metal flow in the runner/gating system for high pressure die casting. Color represents pressures and the diagram on the right shows gate velocities as functions of time.

Another useful result is the pressure drop along the gates, which is necessary to push the metal through the narrow gates. For a given geometry this pressure drop is a function of the filling rate. If pressure needed for a given filling rate is too high for a die casting machine, then the flow rate has to be decreased and/or the total gate area must be increased. In this simulation the pressure drop is about 60 atm, which is not unreasonable.

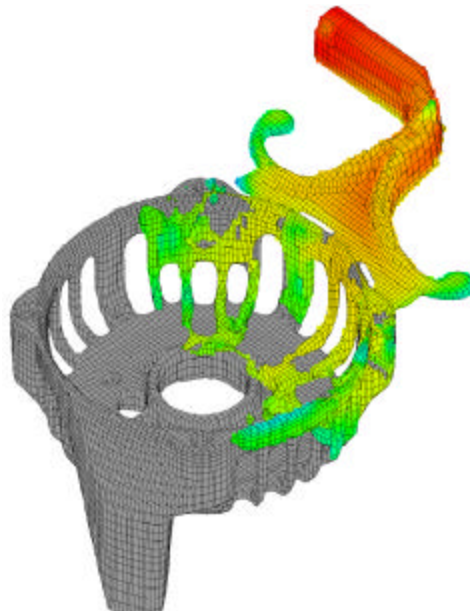


Figure 7. Flow pattern at an early stage of the high pressure filling process. Color denotes temperature.

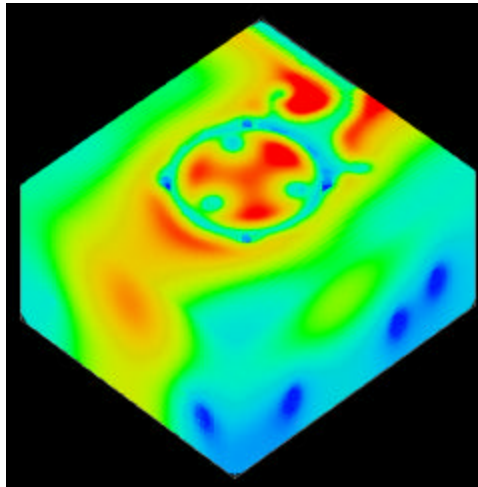


Figure 8. Die temperature distribution after seven thermal cycles

Figure 7 shows a frame from a full 3-D filling simulation with heat transfer. It shows the initial stage of the filling process, when most of the splashing occurs. Air is entrained mainly in the thicker sections of the die cavity, where free surface breakup and flow recirculation are more likely to occur. An examination of the actual part confirmed that assertion. Also confirmed was the prediction that the last section to be filled is the thick mounting bracket that is located opposite to the gates, and where most of the oxide film is accumulated as surface defects.

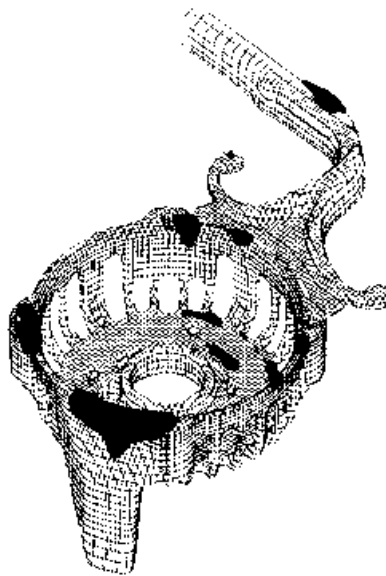


Figure 9. The likely locations of shrinkage porosity in the solidified casting (dark shaded areas).

The filling simulation predicted that the overall solid fraction in the metal at the end of filling was less than 2%, which is acceptable in this case. Other thermal aspects of the process can be analyzed by carrying out a thermal die cycling simulation, where the die is filled, then emptied once the metal had solidified, sprayed and rested. Repeating this process a few times allows engineers to optimize the location of the cooling channels and cycle times, as well as to obtain more realistic temperature distribution in the die for a full filling simulation. Figure 8 shows the temperature distribution in a portion of the die after seven thermal cycles. One can see that the area around the runner, near the symmetry plane, is the hottest.

Finally, predictions were made regarding the location of shrinkage porosity modeling solidification as a continuation to the filling run. Feeding was assumed through the runner/gating system until the metal in the gates froze. This occurred in about 3 *sec* after the end of filling. Figure 9 shows the likely locations of shrinkage porosity. As may be expected, porosity is located mainly in thick, bulky sections.

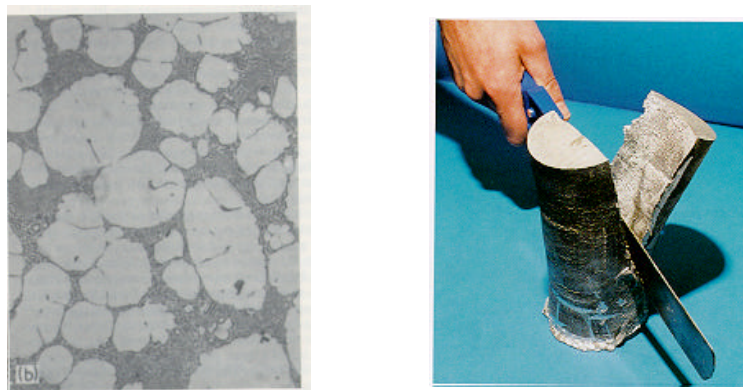


Figure 10. Globular microstructure of semi-solid alloys (left) results in shear thinning behavior (right).

3. *Semi-Solid Metal Processing*

Semi-solid metal processing involves handling specially prepared alloys with globular grain structure. Those alloys in a semi-solid state show shear-thinning behavior that simplifies their handling (Fig. 10). It can be shown that the thixotropic behavior of semi-solid metals can be described with a single transport equation for the apparent viscosity μ , which is a function of solid fraction, shear rate and time [7]:

$$\partial\mu/\partial t + (\mathbf{u}\cdot\nabla)\mu = (\mu_0-\mu)/\tau$$

Here $\mu_0(\dot{\gamma}, f_s)$ is the steady state apparent viscosity, which is a function of the shear rate and solid fraction, \mathbf{u} flow velocity, t time, and τ is the characteristic time.

One of the important issues in modeling thixotropic fluids is quantifying the time-dependence of the apparent viscosity. In the present model, the time dependence is described by characteristic thinning and thickening times. These quantities can be obtained from simple rheological experiments, *e.g.*, hysteresis measurements [8].

Another example is a rapid compression test where a semi-solid slug (36 mm radius and 42 mm height) is compressed between two flat plates [9]. In the example shown in Fig. 11, an A357 semi-solid slug is compressed at the rate of 0.5 m/sec. Comparing the measured and computed total force acting on one of the plates allows us to calibrate the model. As a result, the characteristic thinning time is estimated at about 0.05 sec, in agreement with measurements obtained in step-change experiments in cylindrical rheometers.

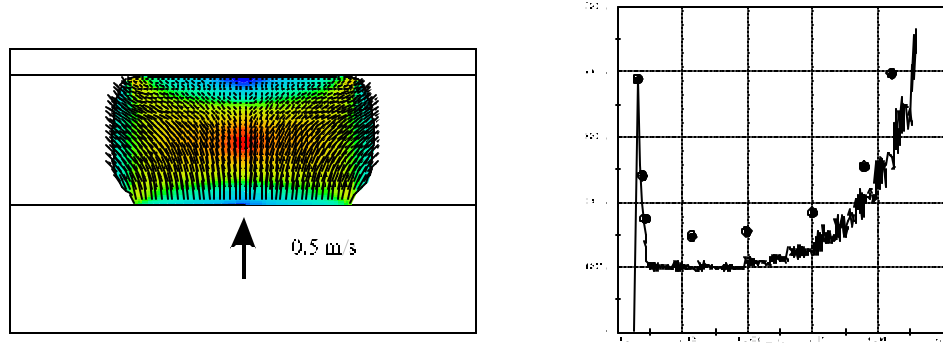


Figure 11. Rapid compression of a semi-solid slug (left). Color denotes strain rate. The total force (N) acting on the top plate is shown on the right as a function of time. Shaded circles show experimental data (from [9]).

This example shows how a simple, but physically sound mathematical model can be useful in interpreting experimental data. The simplicity of the mathematical approach is an advantage since it requires less experimental data to define the model, and also makes it easier to understand the solution.

4. Lost Foam Process

The lost foam casting process offers advantages over the more conventional gravity pour filling method in that the filling in the lost foam process is generally smoother and less coring is needed to cast complex shapes. The challenge in modeling the lost foam process is to accurately describe the dynamics of the metal/foam interface including the evolution of the liquid and gaseous foam decomposition products. The escape of these products from the mold cavity is to a large degree governed by the permeability of the foam coating. Figure 12 shows a schematic of a typical metal/foam interface.

The *FLOW-3D*[®] lost foam model describes foam as a constant temperature obstacle, which may have spatially variable thermal properties. Lighteners (cavities) can be introduced in the foam to speed up the filling process. The foam removal is governed by the rate of heat exchange between the metal and foam, which in turn is defined by a heat transfer coefficient. In fact, the metal/foam heat transfer coefficient is the only parameter that must be defined from experiments (given that all usual material property data is known). The value of that parameter should correlate with the properties of the coating: more permeable coating enables faster escape of the gaseous foam residue, reducing the gap between metal and foam, thus, increasing the heat transfer coefficient.

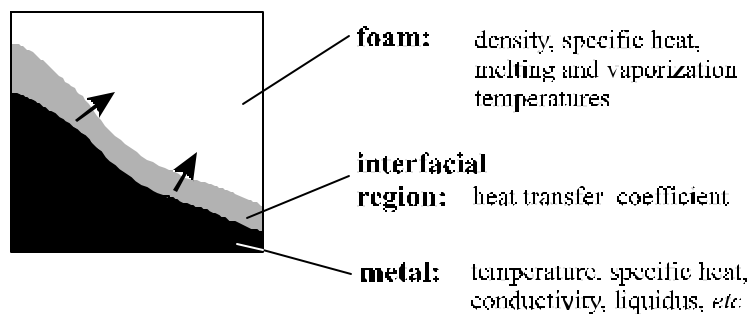


Figure 12. Schematic of the metal/foam interface.

It is very difficult to measure the metal/foam heat transfer coefficient directly. However, its value can be easily estimated by measuring the speed of the metal/foam front or the total filling time. As with the semi-solid metal model, the lost foam model definition is reduced to setting a single ‘free’ parameter. Despite its mathematical simplicity, the lost foam model allows engineers to analyze many important features of this complex process [10].

Important things to investigate in a lost foam process are cold shuts and foam residue entrapment. Cold shuts are an issue because of large heat losses exhibited by the metal while decomposing the foam, while the residue entrapment results in mechanical weaknesses in the solidified casting. Figure 13 shows a simple 2-D flow of aluminum into a rectangular cavity with four cores, initially filled with foam. The average velocity is 0.05 *m/sec*, much smaller than usually encountered in gravity pour castings where velocities up to 3 *m/sec* are common.

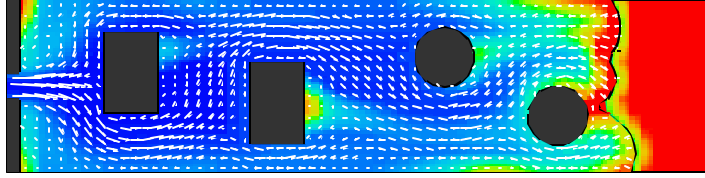


Figure 13. Lost Foam filling process. Liquid metal is entering through the ingate on the left and is colored according to the foam residue content (red denotes high concentration). The intact foam on the right is also colored red.

A residue that forms at the metal/foam interface is tracked by solving a residue transport equation. The simulation shows that the residue is likely to get trapped where two metal fronts meet in wakes of internal obstructions, forming ‘folds’. The simulation also reveals that the metal front temperature drops to the liquidus value very quickly after coming into contact with foam. The large latent heat of aluminum allows the metal to keep flowing, but over 10% of the metal at the end of filling is mushy.

5. *Inclusion Tracking*

Small solid and liquid inclusions in melts can be represented with mass particles. The dynamics of these particles can be computed by solving a particle transport equation in which inertial forces are combined with pressure forces, fluid/particle drag, gravity and diffusion [11]. A number of particles with varying size and mass may be introduced into the flow to describe a spectrum of inclusion.

The particle model is applied below to the continuous casting flow in a titanium hearth (Fig. 14). The liquid metal enters a rectangular bath from the left, from where it flows further into a cylindrical continuous casting mold and leaves it at the bottom at the speed of 10 *mm/sec*. The diameter of the mold is 600 *mm*. The metal is heated from the top by two plasma torches: one above the bath and the other above the mold. At the same time the metal is cooled at the interface with the water-cooled copper hearth. Large temperature gradients develop in the liquid metal that generate a thermal convection and Marangoni type flows. The latter occurs due to temperature variation along the metal free surface that result in surface tension forces tangential to the surface. Those thermally induced flows are much stronger than the overall net flow of metal from the inlet into the mold.

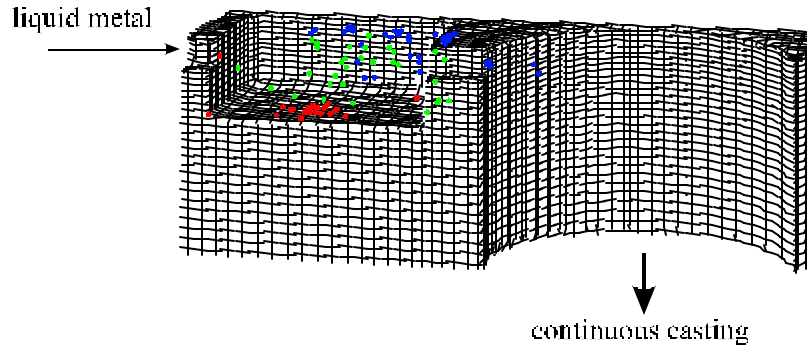


Figure 14. Tracking inclusions in a titanium hearth using the mass particle dynamics model. Blue particles are 10% lighter than metal, green particles have the same density as the metal, and red particles are 10% heavier.

There are three types of inclusions that are present in the incoming flow: light, neutral and heavy. The density of the light and heavy inclusions is assumed to differ by 10% from the density of the fluid. Figure 14 shows the distribution of the particles after about 3 minutes from the start of the simulation. Heavier particles (red) accumulate at the bottom of the bath collected in the middle by the Marangoni flow. The neutral particles are scattered around the bath and the light ones accumulate near the free surface. The simulation shows that these light particles are more likely than other to enter to mold since the mold inlet is located close to free surface. During the actual casting process the light inclusions have to periodically be removed from the free surface by a ladle.

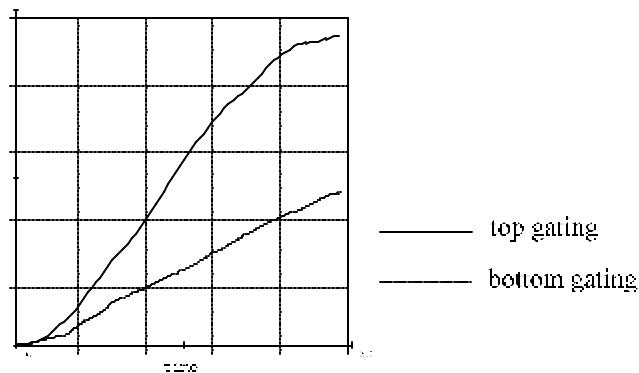


Figure 15. Total amount of oxide produced during top-gated and bottom-gated mold fillings.

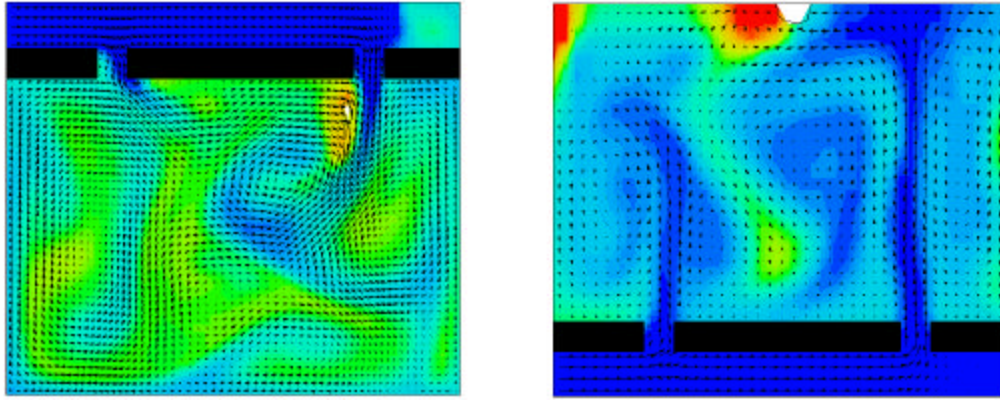


Figure 16. Distribution of surface inclusions (oxides) at the end of filling: top gating (left) and bottom gating (right). Red color denotes higher concentration.

Surface oxides can also be trapped in the liquid metal bulk during filling, as was discussed in the Simple Gating Section. These inclusions represent a more continuous entity that cannot be accurately represented with particles. A surface tracking algorithm, similar to the one described in the Lost Foam Section, can be employed instead, in which the surface defects represent oxide film rather than foam residue.

Let us look again at two of the filling examples presented in the Simple Gating Section (cases *a* and *c*) and see how much oxide film is produced in each case and where it ends up at the end of the filling. Figure 15 shows a comparison of the total amount of oxide (in arbitrary units) for each of the four cases. Clearly, the more splashing occurs during filling the more oxide film is produced. Moreover, splashing promotes oxide film entrapment as shown in Fig. 16. Ideally, the oxide film should be pushed towards the mold walls where it is less likely to cause mechanical defects.

Conclusions

Modern numerical simulation tools allow casting designers and engineers to gain insight into many aspects of the casting process. With the growing complexity of these processes, it is important that the researcher has some understanding of the numerical models that he is trying to use and the physical phenomena that he is attempting to simulate. Such understanding helps to select the right tools and to interpret the results.

Simplifying modeling assumptions, a reduction of the number of parameters needed to define the model also result in more efficient simulations, as was shown in the examples in this paper. These examples were produced using a general-purpose code *FLOW-3D*[®]. *FLOW-3D* has a

library of physical models and numerical approximations, which can be combined to efficiently model a variety of casting processes.

References

1. C.W. Hirt and J.M. Sicilian, "A Porosity Technique for the Definition of Obstacles in Rectangular Cell Meshes," 4-th International Conference on Ship Hydrodynamics, Washington, DC, September 1985.
2. C.W. Hirt and B.D. Nichols, "Volume of Fluid (VOF) Methods for the Dynamics of Free Boundaries," *J. Computational Physics*, **39**, 201-255, 1981.
3. D.B. Kothe and W.J. Rider, "Comments on Modeling Interfacial Flows with Volume-of-Fluid Methods," Los Alamos National Laboratory Report LA-UR-94-3384, 1994.
4. "**FLOW-3D**: Computational Modeling Power for Scientists and Engineers," Flow Science, Inc. report, FSI-87-00-01; see also web site www.flow3d.com.
5. J. Campbell, "Invisible Macrodefects in Castings," *Journal de Physique IV*, **3**, 861-872, 1993.
6. M. Barkhudarov, "High Pressure Die Casting Simulation Using **FLOW-3D**," *Die Casting Engineer*, May/June, p. 36, 1997.
7. M.R. Barkhudarov and C.W. Hirt, "Thixotropic Flow Effects under Conditions of Strong Shear," presented at the "Materials Week '96" TMS Conference, Cincinnati, OH, 7-10 October 1996.
8. M.R. Barkhudarov, C.L. Bronisz and C.W. Hirt, "Three-Dimensional Thixotropic Flow Model," presented at the "Semi-Solid Processing of Alloys and Composites," 4-th International Conference, The University of Sheffield, Sheffield, U.K., pp 110-114 of the proceedings, 19-21 June 1996.
9. P. Kapranos, M.R. Barkhudarov and D.H. Kirkwood, "Modeling of Structural Breakdown During Rapid Compression of Semi-Solid Alloy Slugs," to be presented at the "Semi-Solid Processing of Alloys and Composites" 5-th International Conference, Golden, CO, 23-25 June 1998.
10. C.W. Hirt and M.R. Barkhudarov, "Modeling the Lost Foam Process with Defect Prediction," Flow Science, Inc. technical note #45, FSI-97-00TN45, 1997.
11. M.R. Barkhudarov, "Additions to the Particle Transport and Diffusion Model for **FLOW-3D**," Flow Science, Inc. technical note #42, FSI-95-TN42, 1995.